International Journal of Heat and Mass Transfer 52 (2009) 4449–4458

Contents lists available at ScienceDirect

International Journal of Heat and Mass Transfer

journal homepage: www.elsevier.com/locate/ijhmt

Analytical solutions of fluid flow and heat transfer in parallel-plate micro-channels at high zeta-potentials

A. Elazhary, H.M. Soliman *

Department of Mechanical and Manufacturing Engineering, University of Manitoba, Winnipeg, Man., Canada R3T 5V6

ARTICLE INFO

Article history:
Received 4 December 2008
Received in revised form 18 March 2009
Accepted 18 March 2009
Available online 13 May 2009

Keywords:
Micro-fluidics
Fully developed
Laminar flow
Heat transfer
Parallel-plate micro-channels
High zeta-potentials
Analytical solutions

ABSTRACT

This paper investigates the effect of the EDL at the solid–liquid interface on the liquid flow and heat transfer through a micro-channel formed by two parallel plates. The complete Poisson–Boltzmann equation (without the frequently used linear approximation) was solved analytically in order to determine the EDL field near the solid–liquid interface. The momentum equation was solved analytically taking into consideration the electrical body force resulting from the EDL field and the energy equation was solved analytically taking viscous dissipation into consideration. Effects of the channel size and the strength of the zeta-potential on the electrostatic potential, the streaming potential, the velocity profile, the temperature profile, the volume flow rate, the apparent viscosity, the friction factor, and Nusselt number are presented and discussed. Results of the present analysis, which are based on the complete Poisson–Boltzmann equation, are compared with a simplified analysis that used a linear approximation of the Poisson–Boltzmann equation.

1. Introduction

Micro-fluidic devices are increasingly becoming an attractive alternative to the conventional flow systems because of their compactness and large surface-to-volume ratio. These micro-scale devices are candidates for applications in heat transfer augmentation, micro-electronics and micro-electro-mechanical systems (MEMS), miniaturized chemical reactors and combustors, aerospace, and biomedical systems. Therefore, it is important to enhance our understanding of the relevant phenomena associated with fluid flow and heat transfer in micro-channels.

Due to the small sizes of these micro-channels, some surface phenomena (such as electrostatic forces and surface roughness) become significantly important. The present work is concerned with the effect of the electrostatic force associated with the electric double layer (EDL) on the fluid-flow and heat-transfer characteristics in micro-channels. Almost all solid surfaces have electrostatic charges, positive or negative, with different intensities. The fact that similar charges repel and different charges attract is the reason for the formation of the EDL. Consider a situation of negatively-charged surfaces bounding a micro-channel carrying a pressure-driven liquid. The negative charges of the solid surface attract the positive charges in the liquid, while repelling the negative charges. As a result, a very-thin layer (an order of magnitude of 0.1 nm) is formed adjacent to the walls. This layer is an immobile (static) layer where the attracted charges do not move with the bulk fluid motion due to the strong attraction force between the wall and the charges. Farther away from the wall, another layer is created where the attraction force diminishes and the charges move with the bulk of the flow. This layer is called the diffuse layer and it is much thicker than the static layer. Both layers are called the EDL. The fluid flow under the influence of the pressure gradient pushes the charges in the diffuse layer towards the end of the channel giving rise to an electrical current called the streaming current. Consequently, the potential difference between the two ends of the channel generates an electrical current in the opposite flow direction known as the induction current. At steady-state conditions, a potential difference, namely the streaming potential, is generated between the two ends of the channel. The induction current carries charges and molecules in the opposite direction of the flow creating extra impedance to the flow motion which is called the electro-viscous effect. In some cases, the electro-viscous effect is so strong that it causes a reverse flow near the wall. The maximum strength of the electrostatic charges occurs at the surface and is called the zeta-potential, ξ. The strength of the electrostatic potential, ψ, declines exponentially as we move away from the surface. Because of this exponential decline, the effect of the EDL on the fluid-flow and heat-transfer characteristics is significant only for channels with very small hydraulic diameters, and this effect intensifies as the zeta-potential increases.

* Corresponding author. Tel.: +1 204 474 9307; fax: +1 204 275 7507.
E-mail address: hsolima@cc.umanitoba.ca (H.M. Soliman).

0017-9310/$ - see front matter © 2009 Elsevier Ltd. All rights reserved.
doi:10.1016/j.ijheatmasstransfer.2009.03.036

Nomenclature

a	half distance between the plates (m)
A_c	cross-sectional area of the flow channel (m^2)
Br	Brinkman number
c_p	specific heat ($J\ kg^{-1}\ K^{-1}$)
D_h	hydraulic diameter (m)
e	electron charge (1.6021×10^{-19} C)
E_s	streaming potential (V)
E_z	electric field strength ($V\ m^{-1}$)
f	friction factor
h	convective heat transfer coefficient ($W\ m^{-2}\ K^{-1}$)
I_c	conduction current (A)
I_s	streaming current (A)
k	Debye–Hückel parameter (m^{-1})
k_b	Boltzmann constant ($1.3805 \times 10^{-23}\ J\ mol^{-1}\ K^{-1}$)
k_f	fluid thermal conductivity ($W\ m^{-1}\ K^{-1}$)
L	channel length (m)
n_o	ionic number concentration, (m^{-3})
Nu	Nusselt number
p	pressure (Pa)
Q	volume flow rate ($m^3\ s^{-1}$)
q''	wall heat flux ($W\ m^{-2}$)
Re	Reynolds number
T	absolute temperature (K)
T_m	bulk temperature (K)
T_w	wall temperature (K)
v_o	reference velocity ($m\ s^{-1}$)
v_z	fluid velocity in the z direction ($m\ s^{-1}$)
v_{zm}	cross-sectional mean fluid velocity ($m\ s^{-1}$)
W	channel width (m)
x	cross-stream coordinate (m)
z	stream-wise coordinate (m)
z_v^+, z_v^-	Valence of the positive and negative ions

Greek symbols

α_f	fluid thermal diffusivity ($m^2\ s^{-1}$)
β_1	ratio of the total viscous dissipation to the external heat input
β_2	ratio of the local viscous dissipation to the external heat input
ε	dimensionless dielectric constant
ε_o	permittivity of vacuum ($8.854 \times 10^{-12}\ C\ m^{-1}\ V^{-1}$)
θ	dimensionless temperature
λ_o	electric conductivity ($\Omega^{-1}\ m^{-1}$)
μ	fluid viscosity ($kg\ m^{-1}\ s^{-1}$)
μ_a	apparent viscosity ($kg\ m^{-1}\ s^{-1}$)
ξ	zeta-potential (V)
ρ	electric charge density ($C\ m^{-3}$)
ρ_f	fluid density ($kg\ m^{-3}$)
ψ	electrostatic potential (V)

The existence of the EDL phenomenon has been known for over a century. Debye and Hückel [1] in 1923 linearized the exponential Boltzmann ion energy distribution and solved for the distribution of the electric potential in a solution at low wall potential. Their analysis, now known as the Debye–Hückel approximation, is valid only for situations where the zeta-potential is sufficiently low ($\xi <\sim 25$ mV). Later, Burgreen and Nakache [2] determined the ψ-distribution for electrokinetic flow in parallel-plate micro-channels at high ξ. The ψ-distribution was determined in terms of elliptic integral functions of the first kind. Mala et al. [3] used the Debye–Hückel approximation and solved analytically for the velocity distribution, volume flow rate, and friction factor during fully developed laminar flow in a parallel-plate micro-channel. Li [4] extended the analysis to the geometry of two-dimensional rectangular channels. He determined the ψ-distribution, velocity distribution, and volume flow rate from an analytical linear solution (that used the Debye–Hückel approximation) and a numerical nonlinear solution (that used the complete Poisson–Boltzmann equation). Li noted large deviations between the two solutions, particularly in the region close to the channel walls. Chen et al. [5] investigated the fluid-flow characteristics for developing, pressure-driven, liquid flow in parallel-plate micro-channels. The mathematical model (Poisson–Boltzmann, Nernst–Planck, continuity and Navier–Stokes equations) was solved numerically by means of a finite-volume method. For the micro-tubes geometry, Rice and Whitehead [6] solved for the fully developed, laminar velocity distribution using the Debye–Hückel approximation and noted that, near the wall, the negative electrostatic force caused by the migration of ions can exceed the positive force due to the pressure gradient resulting in a region of back flow near the wall. Levine et al. [7] extended the work in Ref. [6] to conditions of high zeta-potentials. All studies reported in Refs. [1–7] were concerned only with the fluid-flow characteristics without including heat transfer.

More recently, the interest in micro-channel heat sinks and other micro-scale energy systems has motivated studies on the effect of EDL on the thermal behaviour of micro-channels. Mala et al. [8] used the Debye–Hückel linearization to solve analytically for the fully-developed fluid flow in parallel-plate micro-channels. The temperature distribution and Nusselt number for developing heat transfer with uniform wall temperature were obtained by solving the energy equation numerically. The results in Ref. [8] are valid only for conditions of low ξ. A semi-analytical solution was obtained by Yang et al. [9] for steady-state, fully developed, laminar liquid flow and heat transfer in micro-channels with a rectangular cross-section. The solution corresponded to aqueous solutions of low ionic concentration and a solid surface of high zeta-potential, and the results of the fluid-flow and heat-transfer characteristics indicated strong affects by the EDL. Soong and Wang [10] used the Debye–Hückel linearization and solved analytically for the velocity and temperature distributions under hydrodynamically and thermally fully developed flow conditions in a parallel-plate micro-channel with asymmetrical wall-potential and wall-heat-flux conditions. Viscous dissipation was not included in the analysis. Again, these results are expected to be valid only at low ξ. The strong influence of viscous dissipation on the temperature field in micro-channel flows in the absence of electrostatic effects was addressed by Kleinstreuer [11]. It was found that viscous dissipation increases rapidly with a decrease in channel size and that viscous dissipation should be taken into consideration for liquid flow in channels with hydraulic diameters less than 50 μm. Analytical expressions for the temperature distribution and Nusselt number were obtained by Horiuchi and Dutta [12] for the condition of high zeta-potential in parallel-plate micro-channel flow with uniform wall temperature and uniform wall heat flux. However, these solutions corresponded to the assumption of uniform (plug-like) flow velocity. Chakraborty [13] used the Debye–Hückel linearization and solved analytically for the velocity and temperature distributions under hydrodynamically and thermally fully developed flow conditions in a micro-tube with a constant wall heat flux. Viscous dissipation was not included in the analysis and, due to the utilization of the Debye–Hückel linearization, the results are expected to be valid only at low ξ. A numerical solution of the steady, laminar, fully-developed flow (hydrodynamically and thermally) of liquids in a parallel-plate micro-channel was re-

cently proposed by Ngoma and Erchiqui [14] using a slip boundary condition at the walls. The Debye–Hückel linearization was adopted and viscous dissipation was not included.

The objective of the present investigation was to generate analytical solutions for the velocity and temperature distributions during steady, laminar, fully-developed flow (hydrodynamically and thermally) of liquids in parallel-plate micro-channels using the full Poisson–Boltzmann equation and taking the viscous dissipation into consideration. Therefore, the present analysis is expected to be valid for practical situations of high zeta-potentials. A simplified solution that uses the Debye–Hückel approximation was also developed in order to facilitate a quantitative assessment of the effects of this approximation on the fluid-flow and heat-transfer characteristics.

2. Mathematical formulation

The geometry under consideration is shown schematically in Fig. 1, whereby a micro-channel is formed between two parallel plates separated by a distance $2a$. An incompressible Newtonian aqueous 1:1 electrolyte of uniform dielectric constant ε flows in the micro-channel under the influences of an imposed pressure gradient dp/dz and a uniform zeta-potential ξ at both walls. Heat transfer takes place between the walls and the fluid due to a uniform input heat flux q'' imposed at both walls. Solutions for the fluid-flow and heat-transfer characteristics were obtained based on two analyses; a simplified analysis using the Debye–Hückel approximation (see Appendix A) and the more general analysis applicable to high ξ (presented next). The general analysis was conducted under the following assumptions:

(1) The fluid is incompressible and Newtonian with constant thermophysical properties.
(2) The flow is considered to be steady, laminar, and fully developed, both hydrodynamically and thermally.

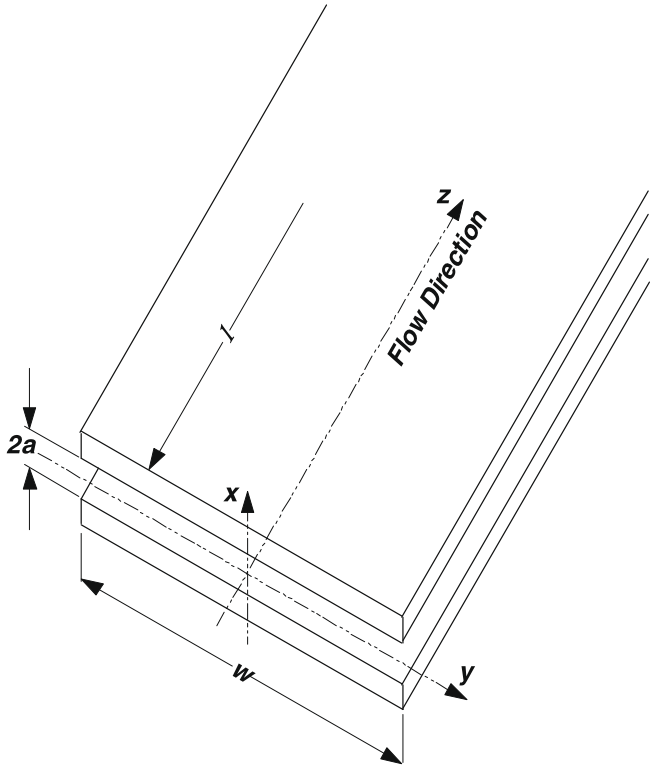

Fig. 1. Geometry and coordinate system.

(3) The channel width (W) is much larger than channel height ($2a$), therefore, the flow is considered to be one-dimensional.
(4) Non-slip conditions apply at both walls.

2.1. Electrostatic potential field

The electrostatic potential field (ψ) in the fluid region is governed by the Poisson–Boltzmann equation, which can be written as [3,5]:

$$\frac{d^2\psi}{dx^2} = \frac{2n_o z_v e}{\varepsilon\varepsilon_o}\sinh\left(\frac{z_v e\psi}{k_b T}\right). \tag{1}$$

The parameters n_o, z_v, e, ε_o, k_b, and T are the bulk concentration of ions, valence of ions, electron charge, permittivity of vacuum, Boltzmann constant, and absolute temperature, respectively. Introducing the following dimensionless parameters:

$$\bar{\psi} = \frac{z_v e\psi}{k_b T}, \quad \bar{x} = \frac{x}{a}, \quad \text{and} \quad k = \left[\frac{2n_o z_v^2 e^2}{\varepsilon\varepsilon_o k_b T}\right]^{\frac{1}{2}}, \tag{2}$$

the dimensionless form of the Poisson–Boltzmann equation can be expressed as

$$\frac{d^2\bar{\psi}}{d\bar{x}^2} = (ka)^2\sinh(\bar{\psi}). \tag{3}$$

The parameter k is the Debye–Hückel parameter and $(1/k)$ is normally referred to as the characteristic thickness of the EDL. Eq. (3) is subject to the following the boundary conditions:

$$\frac{d\bar{\psi}}{d\bar{x}} = 0 \quad \text{at } \bar{x} = 0, \qquad \text{and} \quad \bar{\psi} = \bar{\xi} \quad \text{at } \bar{x} = 1, \tag{4}$$

where, $\bar{\xi} = \frac{z_v e\xi}{k_b T}$.

Integrating Eq. (3) and applying the boundary condition at the center of the channel, we get

$$\frac{d\bar{\psi}}{d\bar{x}} = \sqrt{2}(ka)[\cosh(\bar{\psi}) - \cosh(\bar{\psi}_o)]^{1/2}, \tag{5}$$

where $\bar{\psi}_o$ is the dimensionless electrostatic potential at the center of the channel. Assuming that the half-thickness of the channel is greater than the EDL thickness (i.e., $ka > 1$), we may set the parameter $\bar{\psi}_o$ in Eq. (5) to zero in order to facilitate the integration [12,15]. The lowest value of ka used in the present analysis is 5.5. Integrating Eq. (5), applying the boundary condition at the channel wall, and rearranging, we get

$$\bar{\psi} = 4\tanh^{-1}\left[\tanh\left(\frac{\bar{\xi}}{4}\right)e^{-ka(1-\bar{x})}\right]. \tag{6}$$

The predicted $\bar{\psi} - \bar{x}$ field from Eq. (6) as a function of (ka) and $\bar{\xi}$ will be compared with a numerical solution of Eq. (3) in order to confirm its validity.

2.2. Velocity field

For steady, laminar, one-dimensional flow between parallel plates, the momentum equation (including the effect of EDL) has the following form:

$$\mu\frac{d^2 v_z}{dx^2} - \frac{dp}{dz} + E_z\rho = 0, \tag{7}$$

where ρ is the charge density and it is defined as

$$\rho = -2(n_o z_v e)\sinh\left(\frac{z_v e\psi}{k_b T}\right), \tag{8}$$

and E_z is the electric field strength. The product $E_z\rho$ in Eq. (7) represents an electric body force and its effect appears to be the opposite of that of the pressure gradient. Utilizing the following dimensionless parameters:

$$G_1 = \frac{n_o k_b T}{L\left(-\frac{dp}{dz}\right)}, \quad \bar{v}_z = \frac{v_z}{v_o}, \quad \text{and} \quad \bar{E}_s = \frac{LE_z}{\xi}, \tag{9}$$

where v_o is a reference velocity given by $v_o = \frac{1}{\mu}\left(-\frac{dp}{dz}\right)a^2$. Substituting from Eq. (3), the momentum equation reduces to

$$\frac{d^2\bar{v}_z}{d\bar{x}^2} - \frac{2G_1\bar{\xi}\bar{E}_s}{(ka)^2}\frac{d^2\bar{\psi}}{d\bar{x}^2} + 1 = 0. \tag{10}$$

Eq. (10) is subject to the following boundary conditions:

$$\frac{d\bar{\psi}}{d\bar{x}} = \frac{d\bar{v}_z}{d\bar{x}} = 0 \quad \text{at } \bar{x} = 0, \quad \text{and} \quad \bar{\psi} = \bar{\xi} \quad \text{and} \quad \bar{v}_z = 0 \quad \text{at } \bar{x} = 1. \tag{11}$$

Integrating Eq. (10) twice and imposing boundary conditions (11), the following velocity field was obtained:

$$\bar{v}_z = \frac{1}{2}(1-\bar{x}^2) - \frac{2G_1\bar{\xi}^2\bar{E}_s}{(ka)^2}\left(1 - \frac{\bar{\psi}}{\bar{\xi}}\right), \tag{12}$$

where the electrostatic potential $\bar{\psi}$ is given by Eq. (6). The first term on the right-hand side of Eq. (12) corresponds to the velocity component induced by the pressure gradient and the second term corresponds to the retardation due to the EDL. In order to calculate the velocity from Eq. (12), the streaming potential $\bar{E}_s$ must be determined.

2.3. Streaming potential

The streaming current that is generated due to the transport of charges by the liquid flow can be calculated from the following integral:

$$I_s = \int_{A_c} v_z \rho dA_c. \tag{13}$$

Introducing the dimensionless parameters

$$\bar{\rho} = \frac{\rho}{n_o z_v e} = -2\sinh(\bar{\psi}) \quad \text{and} \quad \bar{I}_s = \frac{I_s}{2v_o n_o z_v e a}, \tag{14}$$

the streaming current equation can be written in the following dimensionless form:

$$\bar{I}_s = -2\int_0^1 \bar{v}_z \sinh(\bar{\psi}) d(\bar{x}). \tag{15}$$

Substituting from Eqs. (6) and (12) and performing the integration, the dimensionless steaming current can be written as

$$\bar{I}_s = (I_1 - I_3) - \left(\frac{4G_1\bar{\xi}\bar{E}_s}{(ka)^2}\right)(I_2 - I_3), \tag{16}$$

where,

$$I_1 = \frac{4}{(ka)^3}\left\{-ka\left[\ln\left(\frac{1+\eta e^{ka}}{1-\eta e^{ka}}\right) + \frac{\eta e^{ka}}{(\eta e^{ka})^2 - 1}\right] + [\mathrm{Li}_2(\eta e^{ka}) - \mathrm{Li}_2(-\eta e^{ka})] - [\mathrm{Li}_2(\eta) - \mathrm{Li}_2(-\eta)]\right\}, \tag{17a}$$

$$I_2 = \frac{8}{ka}\left[\frac{1 - 2\eta e^{ka}\tanh^{-1}(\eta e^{ka})}{(\eta e^{ka})^2 - 1} - \frac{1 - 2\eta\tanh^{-1}(\eta)}{\eta^2 - 1}\right], \tag{17b}$$

$$I_3 = -\frac{4}{ka}\left[\frac{\eta e^{ka}}{(\eta e^{ka})^2 - 1} - \frac{\eta}{\eta^2 - 1}\right], \tag{17c}$$

$$\eta = \tanh(\bar{\xi}/4)e^{-ka}, \tag{17d}$$

and $\mathrm{Li}_2(\beta)$ is the Poly-Logarithmic function of second order defined by

$$\mathrm{Li}_2(\beta) = -\int_0^\beta \frac{\ln(1-t)}{t} dt. \tag{17e}$$

An equilibrium state occurs when the streaming current is equal to the conduction current, i.e.,

$$I_c + I_s = 0, \tag{18}$$

which can be written in the following dimensionless form:

$$\bar{I}_c + \frac{G_2(ka)^2}{\bar{\xi}}\bar{I}_s = 0, \tag{19}$$

where $G_2 = \frac{L\varepsilon\varepsilon_o\left(-\frac{dp}{dz}\right)}{2\mu\lambda_o}$ and the dimensionless conduction current is $\bar{I}_c = \frac{\bar{E}_s\bar{A}_c}{\bar{L}}$. Substituting Eq. (16) into Eq. (19) and rearranging, we get

$$\bar{E}_s = \frac{\frac{G_2(ka)^2}{\bar{\xi}}(I_3 - I_1)}{1 - 4G_1G_2(I_2 - \bar{\xi}I_3)}. \tag{20}$$

2.4. Temperature field

The energy equation for steady-state, laminar, and fully-developed (hydrodynamically and thermally) flow is given by

$$v_z\frac{\partial T}{\partial z} = \alpha_f\left\{\frac{\partial^2 T}{\partial x^2} + \frac{\mathrm{Pr}}{c_p}\left(\frac{dv_z}{dx}\right)^2\right\}, \tag{21}$$

where α_f, c_p, and Pr are the thermal diffusivity, specific heat, and Prandtl number, respectively. The last term in Eq. (21) accounts for the effects of viscous dissipation. Assuming the boundary condition of uniform input heat flux (q'') at both walls of the channel boundary, and performing an overall energy balance, we get

$$\frac{\partial T}{\partial z} = \frac{dT_w}{dz} = \frac{dT_m}{dz} = \frac{q''}{\rho_f v_{zm} c_p a} + \frac{\mu}{\rho_f v_{zm} c_p a}\int_0^a \left(\frac{dv_z}{dx}\right)^2 dx, \tag{22}$$

where v_{zm} is the mean axial velocity in the flow direction. Substituting the value of the axial temperature gradient from Eq. (22) into Eq. (21) and using these dimensionless parameters,

$$\theta = \frac{T_w - T}{(q''a/k)}, \quad \text{and} \quad \mathrm{Br} = \frac{\mu(a^2(-dp/dz)/\mu)^2}{aq''} \tag{23}$$

the energy equation can be written as

$$\frac{d^2\theta}{d\bar{x}^2} + \left(\frac{\bar{v}_z}{\bar{v}_{zm}}\right)\left[1 + \mathrm{Br}\int_0^1 \left(\frac{d\bar{v}_z}{d\bar{x}}\right)^2 d\bar{x}\right] = \mathrm{Br}\left(\frac{d\bar{v}_z}{d\bar{x}}\right)^2, \tag{24}$$

where Br is a modified Brinkman number. Eq. (24), together with Eq. (12) for the velocity profile, indicate that the temperature profile is a function of $\bar{\xi}$, (ka), and Br. The boundary conditions for Eq. (24) are: $\theta = 0$ at $\bar{x} = 1$ and $d\theta/d\bar{x} = 0$ at $\bar{x} = 0$. Defining the parameter $J = \int_0^1 (d\bar{v}_z/d\bar{x})^2 d\bar{x}$, the solution of the energy equation has the form

$$\theta = \mathrm{Br}[E_\theta - (\bar{x}-1)A_\theta - C_\theta] - \frac{1 + \mathrm{Br}J}{\bar{v}_{zm}}[F_\theta - (\bar{x}-1)B_\theta - D_\theta], \tag{25}$$

where

$$J = \frac{1}{3} - \frac{8G_1\bar{\xi}\bar{E}_s}{(ka)^2}\left[\ln\left(\frac{1+\eta e^{ka}}{1-\eta e^{ka}}\right) - \frac{1}{ka}\left[\{\mathrm{Li}_2(\eta e^{ka}) - \mathrm{Li}_2(-\eta e^{ka})\} - \{\mathrm{Li}_2(\eta) - \mathrm{Li}_2(-\eta)\}\right]\right] + \frac{32(G_1\bar{\xi})^2\bar{E}_s^2}{(ka)^3}\left[\frac{1}{1-(\eta e^{ka})^2} - \frac{1}{1-\eta^2}\right], \tag{26}$$

$$A_\theta = \frac{8G_1\bar{\xi}\bar{E}_s}{(ka)^3}[\mathrm{Li}_2(\eta) - \mathrm{Li}_2(-\eta)] + \frac{32(G_1\bar{\xi})^2\bar{E}_s^2}{(ka)^3}\frac{1}{1-\eta^2}, \tag{27}$$

$$B_\theta = \frac{4G_1\bar{\xi}\bar{E}_s}{(ka)^3}[\mathrm{Li}_2(\eta) - \mathrm{Li}_2(-\eta)], \tag{28}$$

$$C_\theta = \frac{1}{12} - \frac{8G_1\bar{\xi}\bar{E}_s}{(ka)^4}\left[ka\{\mathrm{Li}_2(\eta e^{ka}) - \mathrm{Li}_2(-\eta e^{ka})\} - 2\{\mathrm{Li}_3(\eta e^{ka}) - \mathrm{Li}_3(-\eta e^{ka})\}\right] + \frac{16(G_1\bar{\xi})^2\bar{E}_s^2}{(ka)^4}\ln\left[\frac{(\eta e^{ka})^2}{1-(\eta e^{ka})^2}\right], \quad (29)$$

$$D_\theta = \frac{5}{24} - \frac{G_1\bar{\xi}^2\bar{E}_s}{(ka)^2} + \frac{4G_1\bar{\xi}\bar{E}_s}{(ka)^4}[\mathrm{Li}_3(\eta e^{ka}) - \mathrm{Li}_3(-\eta e^{ka})], \quad (30)$$

$$E_\theta = \frac{\bar{x}^4}{12} - \frac{8G_1\bar{\xi}\bar{E}_s}{(ka)^4}\left[ka\bar{x}\{\mathrm{Li}_2(\eta e^{ka\bar{x}}) - \mathrm{Li}_2(-\eta e^{ka\bar{x}})\} - 2\{\mathrm{Li}_3(\eta e^{ka\bar{x}}) - \mathrm{Li}_3(-\eta e^{ka\bar{x}})\}\right] + \frac{16(G_1\bar{\xi})^2\bar{E}_s^2}{(ka)^4}\ln\left[\frac{(\eta e^{ka\bar{x}})^2}{1-(\eta e^{ka\bar{x}})^2}\right], \quad (31)$$

and

$$F_\theta = -\frac{\bar{x}^4}{24} + \frac{\bar{x}^2}{4} - \frac{G_1\bar{\xi}^2\bar{E}_s\bar{x}^2}{(ka)^2} + \frac{4G_1\bar{\xi}\bar{E}_s}{(ka)^4}[\mathrm{Li}_3(\eta e^{ka\bar{x}}) - \mathrm{Li}_3(-\eta e^{ka\bar{x}})]. \quad (32)$$

2.5. Apparent viscosity

The volume flow rate can be calculated from the relation

$$Q = 2W\int_0^a v_z dx = 2Wav_{zm}. \quad (33)$$

In dimensionless form, Eq. (33) can be written as

$$\overline{Q} = \frac{Q}{2aWv_o} = \bar{v}_{zm}, \quad (34)$$

where the mean axial velocity is given by

$$\bar{v}_{zm} = \int_0^1 \bar{v}_z d\bar{x} = \frac{1}{3} + \frac{4G_1\bar{\xi}\bar{E}_s}{(ka)^3}\left[\frac{(ka)\bar{\xi}}{2} + \{\mathrm{Li}_2(\eta e^{ka}) - \mathrm{Li}_2(-\eta e^{ka})\} - \{\mathrm{Li}_2(\eta) - \mathrm{Li}_2(-\eta)\}\right]. \quad (35)$$

For Poiseulle flow between two parallel plates without the EDL effect, the volumetric flow rate is expressed as

$$Q = \frac{2(-dp/dz)a^3W}{3\mu_a}, \quad (36)$$

where μ_a stands for the apparent viscosity. Eq. (36) can be written as

$$\overline{Q} = \frac{\mu}{3\mu_a}. \quad (37)$$

Comparing Eqs. (34) and (37), we get after rearranging

$$\frac{\mu_a}{\mu} = \frac{1}{3\bar{v}_{zm}} = \frac{1}{3\overline{Q}}. \quad (38)$$

2.6. Friction factor

The friction factor is normally defined as

$$f = \frac{2a(-dp/dx)}{\rho_f v_{zm}^2}, \quad (39)$$

and Reynolds number is given by

$$\mathrm{Re} = 4a\rho_f v_{zm}/\mu. \quad (40)$$

Combining Eqs. (39) and (40), and using the definition of G_1 given by Eq. (9), we get

$$f\mathrm{Re} = \frac{8}{\bar{v}_{zm}} = \frac{8}{\overline{Q}} \quad (41)$$

where $\bar{v}_{zm}$ is given by Eq. (35). Since μ_a/μ and f Re are directly proportional to $\overline{Q}$, as given by Eqs. (38) and (41), respectively, only the results of $\overline{Q}$ will be presented later.

2.7. Nusselt number

The formulation for the bulk temperature can be written as

$$T_m = \frac{2W\int_0^a Tc_p\rho_f v_z dx}{\rho_f Qc_p} = \frac{\int_0^a Tv_z dx}{av_{zm}} = \frac{\int_0^1 T\bar{v}_z d\bar{x}}{\bar{v}_{zm}}. \quad (42)$$

Introducing the definition of θ from Eq. (23) into Eq. (42), we get

$$\theta_m = \int_0^1 \theta\left(\frac{\bar{v}_z}{\bar{v}_{zm}}\right)d\bar{x}. \quad (43)$$

Substituting Eq. (25) in Eq. (43) and rearranging, the dimensionless bulk temperature can be expressed as

$$\theta_m = \frac{\mathrm{Br}\int_0^1 G_{v\theta}d\bar{x} - \frac{1+\mathrm{Br}J}{\bar{v}_{zm}}\int_0^1 H_{v\theta}d\bar{x}}{\bar{v}_{zm}}, \quad (44)$$

where

$$G_{v\theta} = \bar{v}_z[E_\theta - (\bar{x}-1)A_\theta - C_\theta], \quad (45)$$

and

$$H_{v\theta} = \bar{v}_z[F_\theta - (\bar{x}-1)B_\theta - D_\theta] \quad (46)$$

Using the definitions of the convective heat transfer coefficient, $h = q''/(T_w - T_m)$, and the hydraulic diameter, $D_h = 4$(area)/wetted perimeter = 4a, Nusselt number can be written as

$$\mathrm{Nu} = \frac{hD_h}{k_f} = \frac{4aq''}{k_f(T_w - T_m)} = \frac{4}{\theta_m} \quad (47)$$

Substituting Eq. (44) in Eq. (47), the following formulation was obtained for Nusselt number

$$\mathrm{Nu} = \frac{4\bar{v}_{zm}}{\mathrm{Br}\int_0^1 G_{v\theta}d\bar{x} + \frac{1+\mathrm{Br}J}{\bar{v}_{zm}}\int_0^1 H_{v\theta}d\bar{x}}. \quad (48)$$

Analytical (closed form) expressions were obtained for the two integrals in Eq. (48). However, these expressions are quite cumbersome and therefore, will not be reproduced here. The value of Nu from the above formulation is dependent on $\bar{\xi}$, (ka), and Br.

For the special case of pure Poiseulle flow (Br = 0 and $\bar{\xi} = 0$), Eq. (12) reduces to $\bar{v}_z = (1-\bar{x}^2)/2$, Eq. (35) reduces to $\bar{v}_{zm} = 1/3$, Eq. (25) reduces to $\theta = 3\left[\frac{\bar{x}^4}{24} - \frac{\bar{x}^2}{4} + \frac{5}{24}\right]$, and Eq. (43) reduces to $\theta_m = 17/35$. Substituting this value of θ_m into Eq. (47), we get the well-known value of Nusselt number for pure Poiseulle flow, Nu = 140/17 = 8.235.

3. Results and discussion

All the results presented in this paper correspond to an infinitely diluted aqueous 1:1 electrolyte solution ($n_o = 6.022\times 10^{20}$ m^{-3}) at $T = 298$ K ($\varepsilon = 80$, $\lambda_o = 1.264\times 10^{-7}$ Ω^{-1} m^{-1}, and $\mu = 0.9\times 10^{-3}$ N s m^{-2}). A fixed pressure gradient was used, $(-dp/dz) = 3\times 10^7$ Pa m^{-1}, while different values of a and ξ were utilized in generating the results.

The zeta-potential is the electric potential at the shear plane separating the thin immobile fluid layer bound to the solid surface from the rest of the liquid. This potential is not measurable directly but it can be calculated using theoretical models and experimentally determined electrophoretic mobility. Beside the surface charge density, the electrophoretic mobility depends on a number of factors, such as the pH of the liquid, the electrolyte concentration (ionic strength), dielectric permittivity of the medium, viscosity, and temperature. Deshiikan and Papadopoulos [16] used the modified Booth equation to calculate the zeta-potential from known experimental values of the electrophoretic mobility and reported ξ-values as high as 244.1 mv in magnitude. This

zeta-potential corresponds to $\bar{\xi} = 9.51$ and therefore, the present results will be limited to the range $0 \leqslant \bar{\xi} \leqslant 10$.

Fig. 2 shows a comparison between three solutions of $\bar{\psi}$-distribution corresponding to $\xi = 240$ mv ($\bar{\xi} = 9.35$) and $a = 1.7$ μm ($ka = 5.54$). The three solutions correspond to the full model given by Eq. (6), the simplified model given by Eq. (A.2) and an accurate numerical solution of Eq. (3) together with boundary conditions (4). The close agreement between the full model and the numerical solution indicates that Eq. (6) produces accurate values of $\bar{\psi}$ throughout the channel at high zeta-potentials, thus confirming that the assumption of $\bar{\psi}_o = 0$ in Eq. (5) does not have a strong influence on the $\bar{\psi}$-distribution. On the other hand, the simplified model corresponding to the Debye–Hückel approximation deviates significantly from the other two sets of results. The two parameters influencing the value of $\bar{\psi}$ are $\bar{\xi}$ and (ka) and the influences of these two parameters are shown in Figs. 3 and 4, respectively. Both the simplified and the full model predict that $\bar{\psi}$ increases with an increase in $\bar{\xi}$ or a decrease in (ka); however, the simplified model overestimates the value of $\bar{\psi}$ in all cases. Significant deviations can be seen between the two models at higher values of $\bar{\xi}$. It is clear from Figs. 3 and 4 that $\bar{\xi}$ is the key parameter in determining the magnitude of the deviation between the two models and that even for a narrow channel with $ka = 5.5$, the deviation can be small if $\bar{\xi}$ is small (e.g., $\bar{\xi} = 2$). The present result showing the simplified model over-predicting ψ at high ξ is consistent with previous results [4].

Variation of the streaming potential, $\bar{E}_s$, with $\bar{\xi}$ and (ka) is shown in Fig. 5. Both the simplified and the full models predict that $\bar{E}_s$ decreases as $\bar{\xi}$ increases or (ka) decreases. An increase in ξ results in more ions being attracted in the double layer and less ions carried downstream by the flowing fluid and thus a lower E_s. Also, a decrease in (ka) decreases the volume between the plates resulting in less ions carried downstream and consequently a lower E_s. Fig. 5 indicates that the simplified solution overestimates the value of $\bar{E}_s$ in all cases, consistent with the overestimation of $\bar{\psi}$ shown earlier. The deviation between the two solutions increases as $\bar{\xi}$ increases.

The velocity distributions predicted by both the simplified and the full models for the range $0 \leqslant \bar{\xi} \leqslant 10$ are shown in Fig. 6 for $ka = 5.5$ and in Fig. 7 for $ka = 40.7$. The profile marked $\bar{\xi} = 0$ represents the velocity component induced by the pressure gradient without EDL retardation. For a very narrow channel ($ka = 5.5$), as

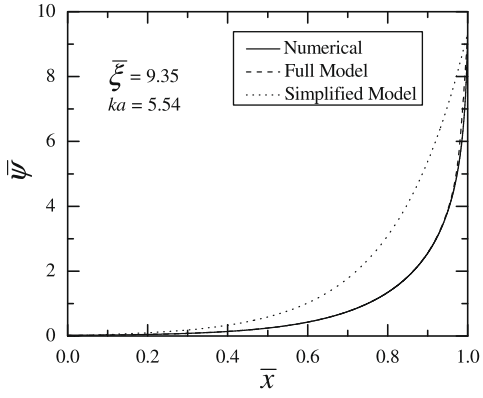

Fig. 2. Validation of Eq. (6) for $\bar{\psi}$.

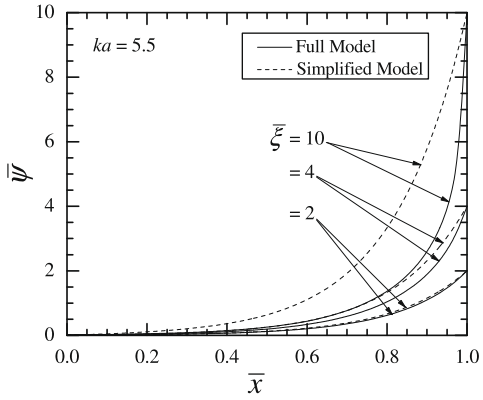

Fig. 3. Effect of $\bar{\xi}$ on $\bar{\psi}$ at $ka = 5.5$.

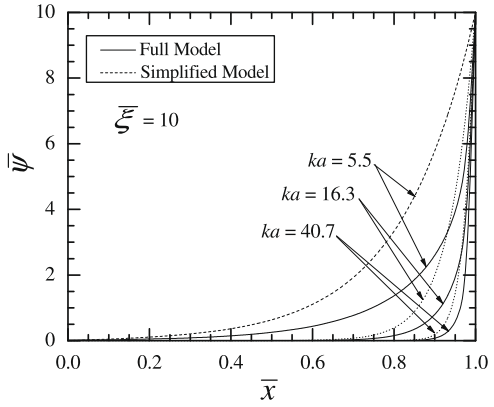

Fig. 4. Effect of (ka) on $\bar{\psi}$ at $\bar{\xi} = 10$.

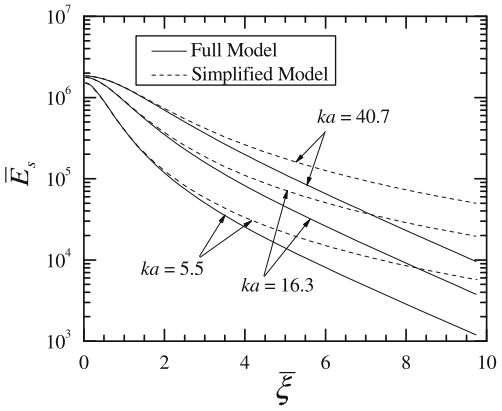

Fig. 5. Variation of $\bar{E}_s$ with $\bar{\xi}$ and (ka).

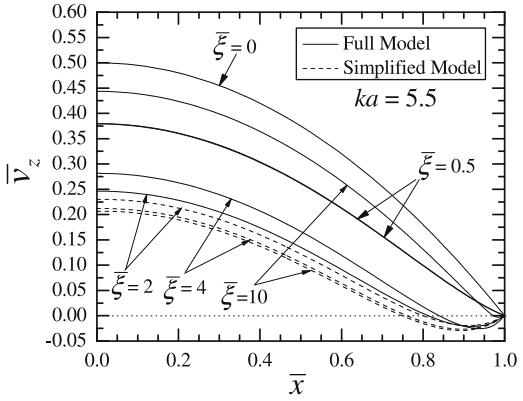

Fig. 6. Velocity profiles for $ka = 5.5$ and various $\bar{\xi}$.

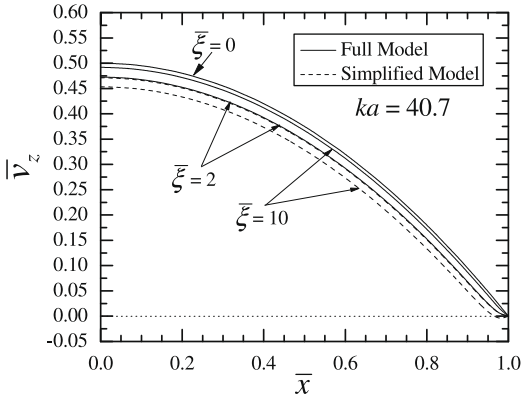

Fig. 7. Velocity profiles for $ka = 40.7$ and various $\bar{\xi}$.

$\bar{\xi}$ increases, Fig. 6 shows that the full model predicts significant retardation of the flow velocity throughout the cross-section and a region of reversed flow near the wall up to $\bar{\xi} = 2$. The deviation between the full and the simplified model is insignificant at $\bar{\xi} = 0.5$ and small at $\bar{\xi} = 2$. Surprisingly, the magnitude of velocity retardation in the core region of the flow decreases as $\bar{\xi}$ increases from 2 to 10, while increased velocity retardation continues near the wall. As well, the near-wall zone (where increasing retardation continues) shrinks in size as $\bar{\xi}$ increases. This result is consistent with the near exponential decrease of $\bar{E}_s$ with $\bar{\xi}$, shown earlier in Fig. 5. It is important to note that the simplified model predicted an opposite trend in terms of the effect of $\bar{\xi}$ on the velocity retardation over the range $2 \leqslant \bar{\xi} \leqslant 10$. For larger channels ($ka = 40.7$), Fig. 7 shows that the velocity retardation is much less significant (percentage-wise) for all values of $\bar{\xi}$. These results are consistent with those of Burgreen and Nakache [2] who reported that the retarding flow is less than 10% of the pressure-induced flow for $ka > 20$, while for $ka = 1.6$, the retarding flow component can be as much as 68% of pressure-induced flow at $\bar{\xi} = 4$. The results in Ref. [4] also indicate that for $ka > 1$, the magnitude of the retarding component decreased as $\bar{\xi}$ increased from 4 to 10.

Predictions of the dimensionless volume flow rate, $\bar{Q}$, are shown in Fig. 8. The full solution predicts that $\bar{Q}$ decreases with $\bar{\xi}$ due to velocity retardation down to a minimum value at about $\bar{\xi} = 2.14$ for $ka = 5.5$ and about $\bar{\xi} = 3.31$ for $ka = 40.7$, and then increases with $\bar{\xi}$. The reduction in volume flow rate due to EDL is more significant for low values of ka; the maximum reduction is about 63% for $ka = 5.5$ and only about 9.6% for $ka = 40.7$. The trends in these results are consistent with the velocity results presented earlier. Variation of μ_a/μ with $\bar{\xi}$ and (ka) can be deduced from the results in Fig. 8 using Eq. (38). The trend of variation in μ_a/μ is opposite to that of $\bar{Q}$ in the sense that an increase in $\bar{Q}$ causes a decrease in μ_a/μ and vice versa. The behavior predicted by the full model of increasing μ_a/μ with $\bar{\xi}$ up to a maximum and then decreasing is consistent with the predictions of Levine et al. [7] for micro-tubes. As well, values of f Re and the trend of its dependence on $\bar{\xi}$ and (ka) can be obtained from Fig. 8 together with Eq. (41).

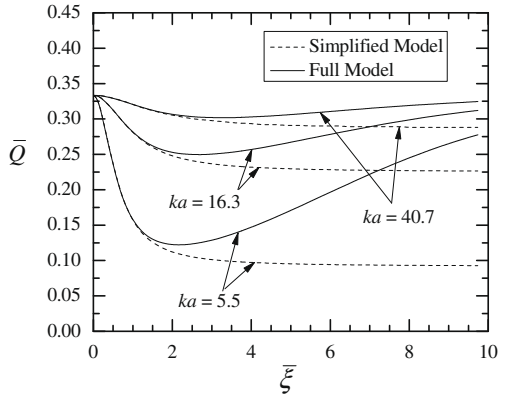

Fig. 8. Variation of $\bar{Q}$ with $\bar{\xi}$ and (ka).

Results of the temperature distribution for $ka = 5.5$, Br = 1, and $0 \leqslant \bar{\xi} \leqslant 10$ are shown in Fig. 9. In all cases, θ increases from zero at $\bar{x} = 1$ to a maximum at $\bar{x} = 0$. The results in Fig. 9 are shown over the range $0 \leqslant \bar{x} \leqslant 0.4$ in order to magnify the core region of the channel. In the core region of the channel, the variation of θ with $\bar{\xi}$ appears to have an irregular trend. Starting from $\bar{\xi} = 0$, the full model predicts a decrease in θ as $\bar{\xi}$ increases to 0.5, then θ increases as $\bar{\xi}$ increases to 4, and then θ decreases as $\bar{\xi}$ increases to 10. The simplified model shows θ decreasing as $\bar{\xi}$ increases to 0.5 (similar to the full model), while $\bar{\xi} = 4$ and 10 result in continuously increasing θ. The deviation between the two models is very small at $\bar{\xi} = 0.5$, but becomes successively larger as $\bar{\xi}$ increases.

In order to explain the trends in Fig. 9, a closer examination was made of energy Eq. (24). According to Eq. (24), θ is dependent on the velocity distribution (which is affected by the EDL), and the viscous dissipation. Generally speaking, θ is expected to increase with a decrease in the velocity and/or an increase in viscous dissipation. Two terms in Eq. (24) that relate to viscous dissipation are $\beta_1 = \mathrm{Br}\int_0^1 (d\bar{v}_z/d\bar{x})^2 d\bar{x}$ and $\beta_2 = \mathrm{Br}(d\bar{v}_z/d\bar{x})^2$, where β_1 is the ratio of the total viscous dissipation within the cross-section to the external heat input, and β_2 is the ratio of the local viscous dissipation to the external heat input. It is the combined effects of β_1, β_2, and v_z that determine the behavior of θ. The variation of β_1 and β_2 with $\bar{\xi}$ at $ka = 5.5$ and Br = 1 is shown in Figs. 10 and 11, respec-

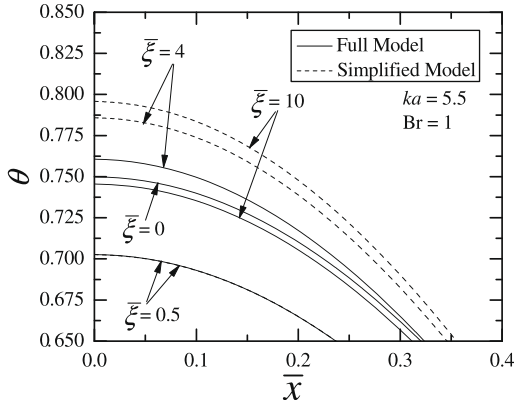

Fig. 9. Temperature profiles for $ka = 5.5$ and Br = 1.

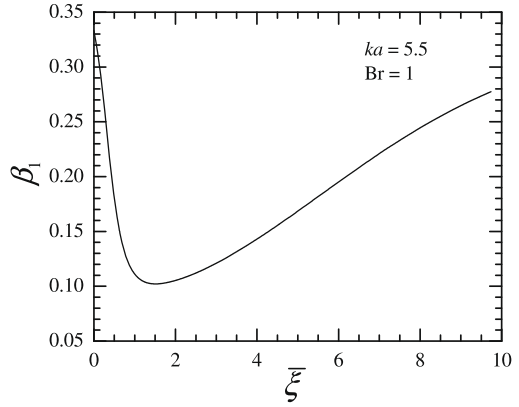

Fig. 10. Variation of β_1 with $\bar{\xi}$ at $ka = 5.5$ and Br = 1.

tively, and the variation of the v_z-profile with $\bar{\xi}$ at $ka = 5.5$ is shown in Fig. 6. It can be seen from Figs. 10 and 11 that both β_1 and β_2 drop significantly, indicating a decrease in viscous dissipation (which causes a decrease in θ), as $\bar{\xi}$ increases from zero to 0.5. On the other hand, Fig. 6 shows that v_z decreases (which causes an increase in θ) as $\bar{\xi}$ increases from zero to 0.5. The net effect in this case is a decrease in θ, as seen in Fig. 9. Going from $\bar{\xi} = 0.5$ to $\bar{\xi} = 4$, β_1, β_2, and v_z continued to decrease; however, the net effect in this case is an increase in θ. Between $\bar{\xi} = 4$ and $\bar{\xi} = 10$, β_1, β_2, and v_z increased and the net effect is a decrease in θ. It must be pointed out that the variations in the magnitude of θ discussed above are small. As well, the accuracy of the results in Fig. 9 was confirmed by an independent numerical solution of the momentum Eq. (10), and energy Eq. (24) that produced very close agreement. The effect of Br on θ is shown in Fig. 12 for $ka = 5.5$ and $\bar{\xi} = 10$. The viscous dissipation increases as Br increases and Fig. 12 shows that θ increases monotonically with Br. A large deviation can be seen between the two models at Br = 10.

The variation of Nusselt number with $\bar{\xi}$ at Br = 1 is shown in Fig. 13 for various values of ka. In all cases, Nu = 7 at $\bar{\xi} = 0$, and as $\bar{\xi}$ increases (with the full model), Nu first increases slightly, then drops to a minimum before rising again. These trends are fully consistent with Eq. (47) and the results in Fig. 9. The simplified model predicts the initial increase in Nu at low $\bar{\xi}$; however, Nu decreases continuously with further increase in $\bar{\xi}$. The deviation between the two models is insignificant for $\bar{\xi} \leqslant 2$, but increases as $\bar{\xi}$ increases. Fig. 14 shows the effect of Br on Nu at $\bar{\xi} = 10$ for various channel widths. For Br < 0.1, the effect of viscous dissipation is insignificant and Nu plateaus at a constant value for all channel widths. For Br > 0.1, θ increases with Br resulting in a decrease in Nu. The two models predict the same trend; however, Fig. 14 shows that the deviation between the two models becomes more significant as ka decreases.

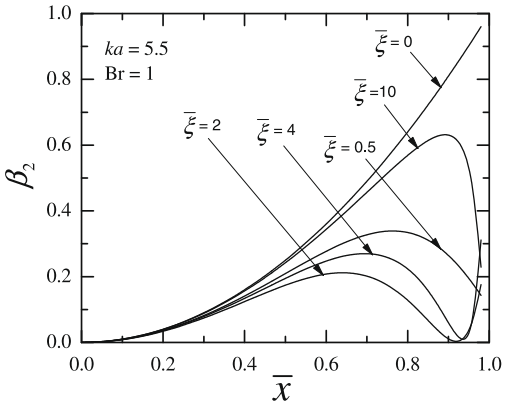

Fig. 11. β_2-profiles for various values of $\bar{\xi}$ with $ka = 5.5$ and Br = 1.

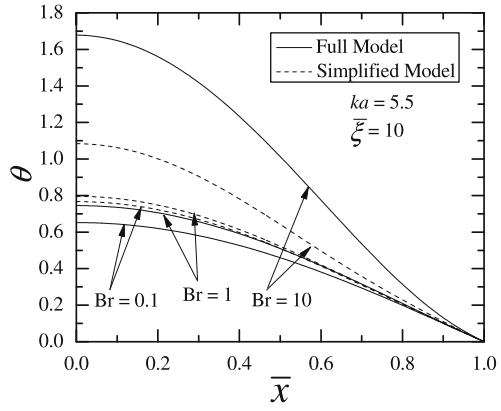

Fig. 12. Effect of Br on the temperature profile for $\bar{\xi} = 10$ and $ka = 5.5$.

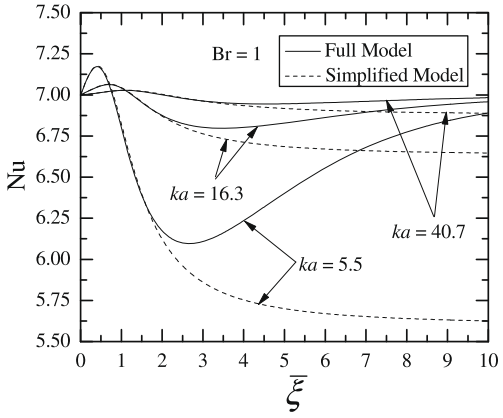

Fig. 13. Variation of Nu with (ka) and $\bar{\xi}$ for Br = 1.

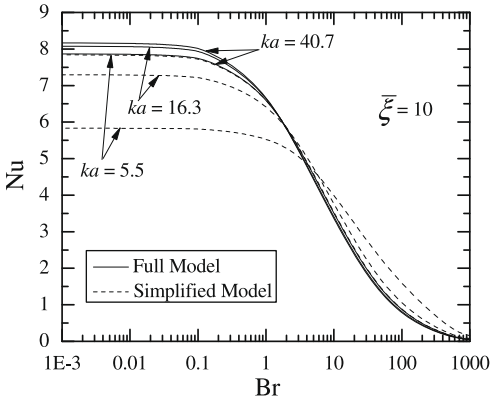

Fig. 14. Effect of Br on Nu at $\bar{\xi} = 10$ for various (ka).

4. Conclusion

An analytical solution was developed for steady, laminar, fully-developed liquid flow and heat transfer in a micro-channel formed by two parallel plates under the influences of an electric double layer (EDL) and viscous dissipation. The solution was based on the full Poisson–Boltzmann equation and the results include the distribution of the electrostatic potential, ψ, the streaming potential, $\bar{E}_s$, the velocity distribution, the temperature distribution, the volumetric flow rate, the apparent viscosity, the friction factor, and Nusselt number. Comparisons were made between the predictions from the present (full) model and those from a simplified model based on the linearized Debye–Hückel approximation. The following conclusions can be drawn from the present results:

1. Both the simplified and the full models predict that $\bar{\psi}$ increases with an increase in $\bar{\xi}$ or a decrease in (ka); however, the simplified model overestimates the value of $\bar{\psi}$ in all cases. The deviations between the two models increase as $\bar{\xi}$ increases.
2. Both the simplified and the full models predict that $\bar{E}_s$ decreases as $\bar{\xi}$ increases or (ka) decreases. The simplified solution overestimates the value of $\bar{E}_s$ in all cases, consistent with the overestimation of $\bar{\psi}$, and the deviation between the two solutions increases as $\bar{\xi}$ increases.

3. The full model predicts that the magnitude of velocity retardation increases as $\bar{\xi}$ increases up to $\bar{\xi} = 2.14$ (for $ka = 5.5$) and $\bar{\xi} = 3.31$ (for $ka = 40.7$), beyond which the velocity retardation decreases with a further increase in $\bar{\xi}$. On the other hand, the simplified model predicts that the velocity retardation increases continuously with $\bar{\xi}$.
4. The full model predicts that the volumetric flow rate decreases as $\bar{\xi}$ increases down to a minimum at $\bar{\xi} = 2.14$ (for $ka = 5.5$) and $\bar{\xi} = 3.31$ (for $ka = 40.7$), beyond which the volumetric flow rate increases with a further increase in $\bar{\xi}$. On the other hand, the simplified model predicts that the volumetric flow rate decreases continuously as $\bar{\xi}$ increases. The trends of the behaviours of the apparent viscosity and the friction factor follow from the trend of the volumetric flow rate.
5. The EDL and the viscous dissipation affect the temperature profile in a complicated manner. The full model and the simplified model predict different trends, and the deviation between the two models increases with $\bar{\xi}$.
6. At Br = 1 and for all values of ka, the full model predicts that Nusselt number initially increases with $\bar{\xi}$, then decreases to a minimum with a further increase in $\bar{\xi}$, and then increases again with $\bar{\xi}$. The variation of Nu with Br is monotonic, with Nu decreasing as Br increases. The predictions from the full and the simplified models are in good agreement up to $\bar{\xi} = 2$, beyond which, the two models deviate in magnitude and trend.

Acknowledgement

The financial assistance provided by the Natural Sciences and Engineering Research Council of Canada (NSERC) is gratefully acknowledged.

Appendix A. Simplified solution

The simplified solution presented in this appendix corresponds to the same geometry, flow conditions, and boundary conditions as the full model presented above, except that the Debye–Hückel approximation is adopted in the simplified model. The hydrodynamics part of this problem has been solved in previous investigations (e.g., [3,8]); however, the thermal aspects presented here (temperature distribution and Nusselt number) are new.

Invoking the Debye–Hückel approximation, the Poisson–Boltzmann equation reduces to

$$\frac{d^2\bar{\psi}}{d\bar{x}^2} = (ka)^2\bar{\psi}. \tag{A.1}$$

The solution of Eq. (A.1), subject to the boundary conditions: $\bar{\psi} = 0$ at $\bar{x} = 0$ and $\bar{\psi} = \bar{\xi}$ at $\bar{x} = 1$, can be found in many references (e.g., [3,8]) as

$$\bar{\psi} = \frac{\bar{\xi}\sinh(ka\bar{x})}{\sinh(ka)}. \tag{A.2}$$

Using solution Eq. (A.2), momentum Eq. (10) can be solved, subject to boundary conditions (11), resulting in the following velocity profile [8]:

$$v_z = \frac{1}{2}(1-\bar{x}^2) - \frac{2\bar{E}_s G_1 \bar{\xi}^2}{(ka)^2}\left[1 - \frac{\sinh(ka\bar{x})}{\sinh(ka)}\right]. \tag{A.3}$$

Using the Debye–Hückel linearization, the streaming current integral in Eq. (15) simplifies to

$$\bar{I}_s = -2\int_0^1 \bar{v}_z\bar{\psi}\,d\bar{x}, \tag{A.4}$$

and an expression can be obtained for the streaming current as [8],

$$\bar{I}_s = -2\alpha\left[\frac{1}{2}(I_4 - I_5) - \frac{2\bar{E}_s G_1\bar{\xi}^2}{(ka)^2}I_6 + \frac{2\bar{E}_s G_1\bar{\xi}^2}{(ka)^2\sinh(ka)}I_7\right], \tag{A.5}$$

where G_1 is defined in Eq. (9), and

$$I_4 = I_6 = \frac{\cosh(ka)-1}{ka}, \tag{A.6}$$

$$I_5 = \left[\frac{1}{ka} + \frac{2}{(ka)^3}\right]\cosh(ka) - \frac{2}{(ka)^2}\sinh(ka) - \frac{2}{(ka)^3}, \tag{A.7}$$

$$I_7 = \frac{1}{2}\left[\frac{1}{ka}\sinh(ka)\cosh(ka) - 1\right], \tag{A.8}$$

and

$$\alpha = \bar{\xi}/\sinh(ka). \tag{A.9}$$

Substituting Eq. (A.5) in Eq. (19) and using the same definitions for G_2 and the conduction current $\bar{I}_c$, the streaming potential can be written as [8]

$$\bar{E}_s = \frac{\alpha\frac{G_2(ka)^2}{\bar{\xi}}(I_4 - I_5)}{1 + 4\alpha G_1 G_2\bar{\xi}\left(I_6 - \frac{I_7}{\sinh(ka)}\right)}. \tag{A.10}$$

The mean velocity based on the profile given by Eq. (A.3) can be formulated as

$$\bar{v}_{zm} = \frac{1}{3} - \frac{2G_1\bar{\xi}^2\bar{E}_s}{(ka)^2}\left[1 - \frac{\cosh(ka)-1}{(ka)\sinh(ka)}\right]. \tag{A.11}$$

The product $f\,\mathrm{Re}$ can be calculated from Eq. (41) with formulation (A.11) for $\bar{v}_{zm}$ resulting in

$$f\mathrm{Re} = \frac{24}{1 - \frac{6G_1\bar{\xi}^2\bar{E}_s}{(ka)^2}\left[1 - \frac{\cosh(ka)-1}{(ka)\sinh(ka)}\right]} = \frac{8}{\bar{Q}} = 24\left(\frac{\mu_a}{\mu}\right). \tag{A.12}$$

The energy equation was solved under the condition of fully-developed flow both hydrodynamically and thermally. Energy Equation Eq. (21) and the temperature distribution given by Eq. (25) are valid; however, the coefficients in Eq. (25) assume the following values:

$$J = \frac{1}{3} - \frac{4\bar{E}_s G_1\bar{\xi}^2}{(ka)^3\sinh(ka)}[(ka)\sinh(ka) - \cosh(ka) + 1] + \frac{2\bar{E}_s^2 G_1^2\bar{\xi}^4}{(ka)^3\sinh^2(ka)}[\sinh(2ka) + 2ka], \tag{A.13}$$

$$A_\theta = \frac{4\bar{E}_s G_1\bar{\xi}^2}{(ka)^3\sinh(ka)}, \tag{A.14}$$

$$B_\theta = \frac{2\bar{E}_s G_1\bar{\xi}^2}{(ka)^3\sinh(ka)}, \tag{A.15}$$

$$C_\theta = \frac{1}{12} - \frac{4\bar{E}_s G_1\bar{\xi}^2}{(ka)^4\sinh(ka)}[ka\cosh(ka) - 2\sinh(ka)] + \frac{\bar{E}_s^2 G_1^2\bar{\xi}^4}{2(ka)^4\sinh^2(ka)}[\cosh(2ka) + 2(ka)^2], \tag{A.16}$$

$$D_\theta = \frac{5}{24} - \frac{\bar{E}_s G_1\bar{\xi}^2}{(ka)^4}[(ka)^2 - 2], \tag{A.17}$$

$$E_\theta = \frac{\bar{x}^4}{12} - \frac{4\bar{E}_s G_1\bar{\xi}^2}{(ka)^4\sinh(ka)}[ka\bar{x}\cosh(ka\bar{x}) - 2\sinh(ka\bar{x})] + \frac{\bar{E}_s^2 G_1^2\bar{\xi}^4}{2(ka)^4\sinh^2(ka)}[\cosh(2ka\bar{x}) + 2(ka)^2\bar{x}^2], \tag{A.20}$$

and

$$F_\theta = \frac{\bar{x}^2}{24}(6 - \bar{x}^2) - \frac{\bar{E}_s G_1\bar{\xi}^2}{(ka)^4}\left[(ka)^2\bar{x}^2 - 2\frac{\sinh(ka\bar{x})}{\sinh(ka)}\right]. \tag{A.21}$$

Finally, Nusselt number was calculated from Eq. (48) with $G_{v\theta}$ and $H_{v\theta}$ given by Eqs. (45) and (46), respectively, with formulation (A.11) for $\bar{v}_{zm}$ and formulations (A.14) to (A.21) for A_θ to F_θ.

References

[1] P. Debye, E. Hückel, Zur theorie der elektrolyte. I. Gefrierpunktserniedrigung und verwandte erscheinungen, Phys. Z. 24 (1923) 185–208.

[2] D. Burgreen, F.R. Nakache, Electrokinetic flow in ultrafine capillary slits, J. Phys. Chem. 68 (1964) 1084–1091.

[3] G.M. Mala, D. Li, C. Werner, H.-J. Jacobasch, Y.B. Ning, Flow characteristics of water through a microchannel between two parallel plates with electrokinetic effects, Int. J. Heat Fluid Flow 18 (1997) 489–496.

[4] D. Li, Electro-viscous effects on pressure-driven liquid flow in microchannels, Colloids Surf. A: Physicochem. Eng. Aspects 195 (2001) 35–57.

[5] X.Y. Chen, K.C. Toh, J.C. Chai, C. Yang, Developing pressure-driven liquid flow in microchannels under the electrokinetic effect, Int. J. Eng. Sci. 42 (2004) 609–622.

[6] C.L. Rice, R. Whitehead, Electrokinetic flow in a narrow cylindrical capillary, J. Phys. Chem. 69 (1965) 4017–4023.

[7] S. Levine, J.R. Marriott, G. Neale, N. Epstein, Theory of electrokinetic flow in fine cylindrical capillaries at high zeta-potentials, J. Colloid Interface Sci. 52 (1975) 136–149.

[8] G.M. Mala, D. Li, J.D. Dale, Heat transfer and fluid flow in microchannels, Int. J. Heat Mass Transfer 40 (1997) 3079–3088.

[9] C. Yang, D. Li, J.H. Masliyah, Modeling forced liquid convection in rectangular microchannels with electrokinetic effects, Int. J. Heat Mass transfer 41 (1998) 4229–4249.

[10] C.Y. Soong, S.H. Wang, Theoretical analysis of electrokinetic flow and heat transfer in a microchannel under asymmetric boundary conditions, J. Colloid Interface Sci. 265 (2003) 202–213.

[11] J. Koo, C. Kleinstreuer, Viscous dissipation effects in microtubes and microchannels, Int. J. Heat Mass Transfer 47 (2004) 3159–3169.

[12] K. Horiuchi, P. Dutta, Joule heating effects in electroosmotically driven microchannel flows, Int. J. Heat Mass Transfer 47 (2004) 3085–3095.

[13] S. Chakraborty, Analytical solutions of Nusselt number for thermally fully developed flow in microtubes under a combined action of electroosmotic forces and imposed pressure gradients, Int. J. Heat Mass Transfer 49 (2006) 810–813.

[14] G.D. Ngoma, F. Erchiqui, Heat flux and slip effects on liquid flow in a microchannel, Int. J. Therm. Sci. 46 (2007) 1076–1083.

[15] P. Dutta, A. Beskok, Analytical solution of combined electroosmotic/pressure driven flows in two-dimensional straight channels: finite Debye layer effects, Anal. Chem. 73 (2001) 1979–1986.

[16] S.R. Deshiikan, K.D. Papadopoulos, Modified Booth equation for the calculation of zeta potential, Colloid Polym. Sci. 276 (1998) 117–124.